THE GEOLOGICAL SOCIETY OF AMERICA®

Latest Permian to Middle Triassic redox condition variations in ramp settings, South China: Pyrite framboid evidence

Yuangeng Huang[1], Zhong-Qiang Chen[1,†], Paul B. Wignall[2], and Laishi Zhao[3]

[1]*State Key Laboratory of Biogeology and Environmental Geology, China University of Geosciences (Wuhan), Wuhan 430074, China*

[2]*School of Earth and Environment, University of Leeds, Leeds LS2 9JT, UK*

[3]*State Key Laboratory of Geological Process and Mineral Resources, China University of Geosciences (Wuhan), Wuhan 430074, China*

ABSTRACT

A detailed, 10 m.y. redox history of Changhsingian to Anisian (latest Permian to Middle Triassic) oceans in ramp settings is reconstructed based on framboidal pyrite analysis from South China. The result shows that the well-established phenomenon of intense ocean euxinia-anoxia is faithfully recorded in pyrite framboid data. Three major euxinia-anoxia episodes, namely, the end-Changhsingian to end-Smithian, middle to late Spathian, and early to middle Anisian, have been recognized from the ramp successions. The first reducing episode is subdivided into four subepisodes: Permian-Triassic boundary, Griesbachian-Dienerian boundary, earliest Smithian, and end-Smithian. Redox variations broadly track other oceanographic proxies. Euxinia-anoxia episodes coincide with positive excursions of conodont ΩCe anomalies, negative excursions of $\delta^{34}S_{cas}$ (carbonate-associated sulfate), increases in sea-surface temperature, and negative excursions of $\delta^{13}C$ in most cases. However, euxinia-anoxia near the Dienerian-Smithian boundary coincided with positive excursions of $\delta^{13}C$ and a general cooling period. This exception may be the result of locally developed water-column anoxia. The Permian-Triassic boundary subepisode witnessed two ephemeral euxinia-anoxia events separated by a dysoxic to oxic period. The former, together with a rapid increase in sea-surface temperature (up to 8 °C), may have been responsible for the biodiversity crisis, while the latter anoxic event destroyed ecosystem trophic structures. In addition to the Permian-Triassic boundary euxinia-anoxia event, which spread over habitats in all oceans, the Spathian and Anisian euxinia-anoxia episodes also prevailed in global oceans. Variation of the oxygen minimum zone are suggested as the driving mechanism that facilitated the movement of oxygen-poor water columns in various paleogeographic settings over this critical period.

INTRODUCTION

Marine ecosystems suffered severe degradation in the latest Permian mass extinction, with over 90% of marine species being wiped out (Erwin, 2006). It has been suggested that the ecosystem did not fully recover until the early Middle Triassic, ~8–9 m.y. after the crisis (Chen and Benton, 2012; Wignall, 2015). Such a long, protracted biotic recovery process is believed to have resulted, in part, from the effects of repeated environmental stresses during the Early Triassic (Hallam, 1991; Payne and Clapham, 2012; Sun et al., 2012; Romano et al., 2013; H.J. Song et al., 2014). In particular, recurring ocean anoxia has been proposed as a key element responsible for the prolonged delay in marine biotic recovery (Hallam and Wignall, 1997; Knoll et al., 2007; Algeo et al., 2011a; Grasby et al., 2013; H.J. Song et al., 2014).

Various geochemical and paleoecologic proxies have been employed to reconstruct the marine redox history, such as authigenic uranium concentrations, iron concentrations, cerium anomalies, molybdenum isotopes, uranium isotopes, sulfur isotopes, carbon isotopes, framboidal pyrite petrography, and biomarkers (e.g., Wignall and Twitchett, 1996, 2002; Isozaki, 1997; Wignall and Newton, 2003; Newton et al., 2004; Grice et al., 2005; Kaiho et al., 2006, 2012; Riccardi et al., 2006, 2007; Algeo et al., 2007, 2008; Gorjan et al., 2007; Xie et al., 2007; Brennecka et al., 2011; Shen et al., 2007, 2011, 2015; Takahashi et al., 2009, 2013, 2014, 2015; Zhou et al., 2012; Proemse et al., 2013; Dustira et al., 2013; H.Y. Song et al., 2013, 2014; Chen et al., 2015; Schoepfer et al., 2015). These studies, however, focused mostly on the Permian-Triassic transition, and only a few papers have addressed marine redox history through the entire Early Triassic (Wignall et al., 2010; Grasby et al., 2013; Song et al., 2012; H.Y. Song et al., 2013, 2014; L. Tian et al., 2014), and fewer still have looked at the Middle Triassic (Song et al., 2012).

Diverse geochemical proxies are powerful tools for reconstructing redox history, but many are easily affected by diagenesis and thus require fresh, unaltered samples. In contrast, even when affected by later diagenetic overgrowths, the original framboidal morphology can still be distinguished. After overgrowth, pyrite framboids become sunflower-like pyrite aggregates, and the boundary between original framboidal pyrite and the overgrowth rim is very distinct (Fig. DR1[1]). Furthermore, surface weathering, a major issue in most geochemical studies, does not affect framboid analysis because the pyrite is converted to iron oxyhydroxides while preserving the original morphology (Lüning et al., 2003; Bond and Wignall, 2005). Framboid size data have been successfully employed to reconstruct redox conditions in both modern and ancient sediments (Bond and Wignall, 2010) and work well in both carbonate and mudstone/shale facies sediments (L. Tian et al., 2014).

In order to build a detailed redox history during mass extinction and the subsequent aftermath, we assessed both size distributions and morphologies of framboidal pyrites from four sections, namely, Meishan, West Pingdingshan, South Majiashan, and Qingyan (Fig. 1), spanning the interval from the latest Permian to Anisian (early Middle Triassic) in South China. Reconstruction of a high-resolution redox history allows us to investigate the temporal link between ocean anoxia and biotic and environmental extremes through this critical period of biotic evolution.

†zhong.qiang.chen@cug.edu.cn

[1]GSA Data Repository item 2016295, analytical results of pyrite framboid sizes and framboid morphologies, is available at http://www.geosociety.org/pubs/ft2016.htm or by request to editing@geosociety.org.

GSA Bulletin; January/February 2017; v. 129; no. 1/2; p. 229–243; doi: 10.1130/B31458.1; 10 figures; Data Repository item 2016295; published online 18 October 2016.

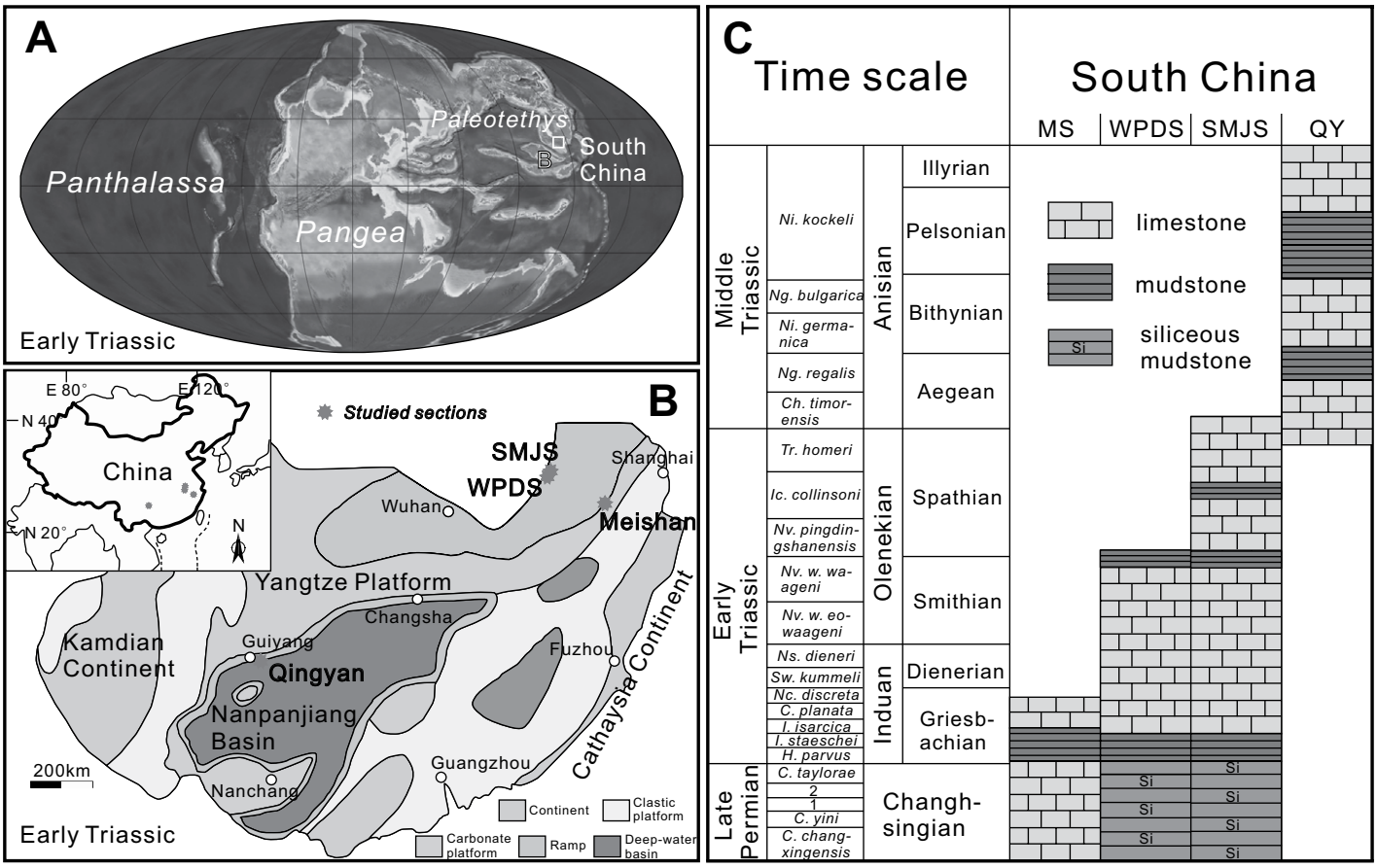

Figure 1. (A) Early Triassic global paleogeographic configuration (base map courtesy of R. Blakey: http://www2.nau.edu/rcb7/240moll.jpg). (B) Early Triassic paleogeographic map of South China showing the study sites (base map modified from Feng et al., 1997). Inset: Location map of China. (C–D) Simplified chronostratigraphic and lithostratigraphic framework through the latest Permian to Middle Triassic of the four studied sections. Abbreviations of the studied sections: MS—Meishan, WPDS—West Pingdingshan, SMJS—Southern Majiashan, QY—Qingyan. 1—*Clarkina meishanensis* Zone, 2—*Hindeodus changxingensis* zone.

GEOLOGICAL AND STRATIGRAPHIC SETTINGS

During the Permian-Triassic transition, South China was located near the equator in the eastern Paleotethys Ocean (Fig. 1A), and two structural highs, namely, the Kongdian and Cathaysia landmasses, were situated in its western and southeastern parts. The Nanpanjiang Basin and South China Northern Marginal Basin were found between these landmasses and were separated by the extensive Yangtze Platform in Early to Middle Triassic times (Fig. 1B). A broad ramp and a narrow ramp were situated at the northern and southern margins of the Yangtze Platform, respectively. Narrow siliciclastic shallow seas fringed the landmasses, and elsewhere carbonates developed in platform, ramp, and basin areas (Feng et al., 1997; Fig. 1B). The selected four study sites were all situated in ramp settings during the Early to Middle Triassic (Fig. 1B). The marine Permian-Triassic boundary beds and Lower Triassic successions are both complete and extensive on the South China block, making this one of the best regions for studying biotic, environmental, and climatic variations during the turnover across the Permian-Triassic transition (Chen and Benton, 2012).

Size distributions and morphologies of pyrite framboids are here documented and analyzed from the uppermost Permian to lower Middle Triassic of four ramp facies sections, namely, Meishan, West Pingdingshan, South Majiashan, and Qingyan in South China (Fig. 1).

Meishan Section

The pyrite framboid samples across the Permian-Triassic boundary were collected from the intensively studied Meishan section, which crops out in Changxing County, ~300 km west of Shanghai City, eastern China (Fig. 1B). This section is not only the global stratotype section and point (GSSP) for the Permian-Triassic boundary, which is placed in the middle of Bed 27 (Yin et al., 2001), but it also has the best documented record of extinction losses and environmental conditions (e.g., Chen et al., 2015). The uppermost Permian succession is composed of thin-bedded limestone of the upper Changxing Formation, while the lowest Triassic sediments are dominated by alternations of thin-bedded marlstone and mudstone with numerous clay ash layers of the Yinkeng Formation. Integration of lithofacies and paleoecologic features shows that the Permian–Triassic succession represents a deepening-up cycle with depositional settings ranging from upper ramp to lower ramp or offshore shelf (Chen et al., 2007, 2015; S. Tian et al., 2014).

Recently, Chen et al. (2015) updated the conodont zonation from the uppermost Changxing and Yinkeng Formations in Meishan. The new conodont zones (with their lithostratigraphic ranges in brackets) include *Clarkina changxingensis* zone (Beds 22–23), *Clarkina yini* zone

(Bed 24), *Clarkina meishanensis* zone (Bed 25), *Hindeodus changxingensis* zone (Bed 26), *Clarkina taylorae* zone (Bed 27a–b), *Hindeodus parvus* zone (Bed 27c–d), *Isarcicella staeschei* zone (Beds 28–29a), *Isarcicella isarcica* zone (Bed 29b), *Clarkina planata* zone (Beds 30–54), and *Neoclarkina discreta* zone (Bed 35 and above). The eight conodont zones from the Permian-Triassic boundary beds enable high-resolution correlations with sections throughout China (Jiang et al., 2007; Zhang et al., 2007, 2014; Chen et al., 2015).

West Pingdingshan Section

Both the West Pingdingshan and South Majiashan sections are situated in a southeastern suburb of Chaohu City, Anhui Province, South China. The Chaohu area was part of the Lower Yangtze Platform ramp during the Early Triassic (Feng et al., 1997; Fig. 1B), and it records a wide range of relatively deep-water settings from epicontinental basin to inner and outer ramp (Chen et al., 2011; M. Li et al., 2016). The Permian-Triassic boundary beds and the lower part of the Lower Triassic succession are well exposed on the western slope of Pingdingshan Hill, while the upper Lower Triassic succession is better exposed 2 km away on the southern slope of Majiashan Hill. The West Pingdingshan section (Fig. 1C) records one of the most complete and best-known Induan-Olenekian boundary successions in China (Zhao et al., 2007).

The Lower Triassic strata exposed at West Pingdingshan consist of the Yinkeng and Helongshan Formations and the basal Nanlinghu Formation. The Yinkeng Formation is composed of greenish/black shale interbedded with marlstone (Beds 3–37), while the Helongshan Formation is characterized by interbeds of thin-bedded dolomitic limestone and calcareous mudstone (Beds 38–53). The lower Nanlinghu Formation is composed of medium-bedded limestone interbedded with a few thin mudstone layers (Beds 54–58). Conodont zones and ammonoid assemblages are well established in this section (Fig. 2; Zhao et al., 2007). The Griesbachian to early Spathian successions yielded the *Hindeodus typicalis*, *Neoclarkina krystyni*, *Sweetospathodus kummeli*, *Neospathodus dieneri*, *Novispathodus waageni eowaageni*, *Novispathodus waageni waageni*, *Novispathodus pingdingshanensis*, and *Triassospathodus homeri* conodont zones; the *Ophiceras-Lytophiceras*, *Prionolobus-Gyronites*, *Flemingites-Euflemingites*, *Anasibirites*, and *Columbites-Tirolites* ammonite assemblages; and the *Claraia stachei–Claraia aurita* and *Eumorphotis inaequicostata–Eumorphotis huancangensis* bivalve assemblages (Tong et al., 2003, 2004; Zhao et al., 2007, 2008).

South Majiashan Section

The Spathian succession of the Nanlinghu Formation is well seen in the South Majiashan section (Fig. 1C). The lower Nanlinghu Formation is composed of medium- to thick-bedded limestone showing large ripples and wavy cross-bedding. The middle Nanlinghu Formation is characterized by thin- to medium-bedded limestone with *Gyrochorte* and *Thalassinoides*, and marine reptile and fish assemblages (Chen et al., 2011; Motani et al., 2014, 2015; Jiang et al., 2014). The upper Nanlinghu Formation consists of medium- to thick-bedded muddy limestone and dolomite, with microbial mats in the uppermost portion of the formation (Zhao et al., 2007; Chen et al., 2011; M. Li et al., 2016). Conodonts of the *Novispathodus pingdingshanensis*, *Triassospathodus homeri*, and *Neospathodus anhuiensis* zones, ammonoids of the *Columbites-Tirolites* and *Subcolumbites* assemblages, and bivalves of the *Guichiella angulata* and *Periclaraia circularis* assemblages are present in the Nanlinghu Formation. Conodont zones established from the lower part of the section correlate well with the same biozones recognized from the uppermost part of the West Pingdingshan section (Zhao et al., 2007, 2008).

Qingyan Section

The Middle Triassic samples were collected from the Qingyan section, which is located in the Huaxi District, 30 km south of Guiyang, the capital city of Guizhou Province, South China. During Early to Middle Triassic, the Qingyan area was situated on a ramp between the Yangtze Platform in the north and the Nanpanjiang Basin in the south (Feng et al., 1997; Fig. 1B). This ramp zone was ~400 km long and 25–70 km wide, and it formed an S-shaped belt, aligned northeast to southwest, that separated a shallow carbonate platform from a deep basin of mixed carbonate and clastic facies in southern Guizhou areas (Feng et al., 1997). The uppermost Permian to Middle Triassic succession is exposed continuously in Qingyan (J. Chen et al., 2010a).

The uppermost Spathian to upper Anisian succession in Qingyan was sampled (Fig. 1C). The uppermost Spathian rocks are assigned to the upper Anshun Formation. The lower part of the exposed succession is dominated by vermicular limestone (a micritic limestone with densely packed, small *Planolites* that give the rock a "wormlike" appearance), while the upper part consists of dolomitic limestone. Conodonts from these two units indicate the *Tr. homeri* zone is present (Ji et al., 2011). In addition, bivalves (*Eumorphotis* cf. *inaequicostata*, *Pteria* cf. *murchisoni*, *Entolium discites*, *Mysidiopteria* cf. *striosus*, *Claraia* sp., *Entolium* sp., and *Leptochondria* sp.), ammonoids (*Tirolites* sp. and *Prophychitoides* sp.), and brachiopods (?*Crurithyris* sp. and ?*Septaliphoria* sp.) are also abundant and corroborate the Spathian age assignment (J. Chen et al., 2010b).

The Anisian Qingyan Formation is subdivided into five members: the Xiaoshan, Mafengpo, Yingshangpo, Leidapo, and Yuqing Members (J. Chen et al., 2010b). Of these, the Xiaoshan Member is dominated by gray, medium-bedded micrite, calcareous mudstone, and bioclastic limestone, and it yields conodonts of the *Chiosella timorensis* zone and diverse ammonoids, bivalves, brachiopods, and gastropods, all of which indicate an earliest Anisian age (Yao et al., 2004; J. Chen et al., 2010b; Ji et al., 2011; Yan et al., 2015). The Mafengpo Member is characterized by dark mudstone interbedded with numerous limestone layers, while the Yingshangpo Member consists of thin- to medium-bedded bioclastic limestone interbedded with yellowish mudstone. These two members yield abundant conodonts, ammonoids, bivalves, brachiopods, gastropods, and echinoids (J. Chen et al., 2010b; Ji et al., 2011). Of these, conodonts are assignable to the *Neogondolella* cf. *bulgarica* zone of early to middle Anisian age (Ji et al., 2011).

The Leidapo Member is composed of yellow mudstone interbedded with thin-bedded limestone with brachiopod-bearing concretions that increase in abundance up section. The uppermost Leidapo Member is well exposed at the so-called Fossil Hill and is dominated by marly and sometimes silty mudstones (J. Chen et al., 2010b). This member is abundantly fossiliferous and contains calcareous algae, ammonoids, annelids, bivalves, brachiopods, bryozoans, cnidarians, conodonts, corals, crinoids, echinoids, foraminifers, gastropods, nautiloids, ostracods, scaphopods, and sponges (Z.Q. Chen et al., 2010; J. Chen et al., 2010a, 2010b). Of these, age-diagnostic ammonoid genera (*Bulogites*, *Acrochordiceras*, *Proarcestes*, *Rieppelites*, *Judicarites*, *Ptychites*, and *Gosauites*) constrain the Leidapo Member to the middle–late Anisian (Stiller and Bucher, 2008, 2011). The overlying Yuqing Member consists of dolomitic limestone and yields ammonoids of late Anisian age (Stiller and Bucher, 2008, 2011).

MATERIALS AND METHODS

We studied 48, 55, and 86 sedimentary rock samples from the West Pingdingshan, South Majiashan, and Qingyan sections, respectively. In addition, the analytical results of pyrite framboids obtained recently from the Meishan sec-

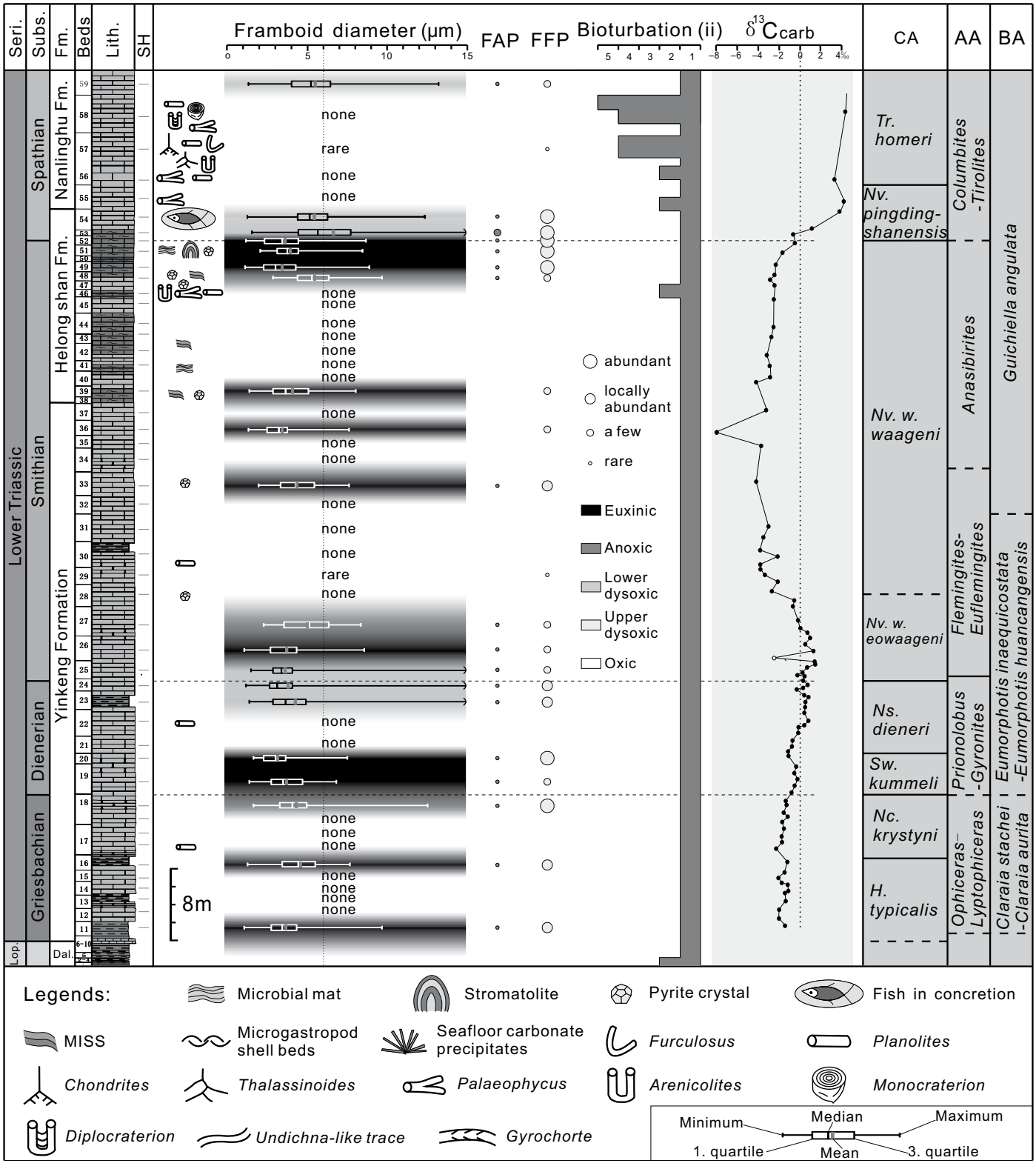

Figure 2. Griesbachian to early Spathian (Early Triassic) paleoredox condition changes from the West Pingdingshan (WPDS) section. Carbon isotope data are after Tong et al. (2007), trace fossil data are after Chen et al. (2011), conodont zonation are after Zhao et al. (2007), and ammonoid and bivalve assemblages are after Tong et al. (2003, 2004). Seri.—Series, Subs.—Substage, Fm.—Formation, Lith.—lithology, SH—sample horizon, FAP—frequency of authigenic pyrite, FFP—frequency of framboid pyrite, ii—ichnofabric index, CA—conodont zonation, AA—ammonoid assemblage, BA—bivalve assemblage, Lop.—Lopingian, Dal.—Dalong Formation, MISS—microbially induced sedimentary structure. Abbreviations: *H.—Hindeodus*, *Nc.—Neoclarkina*, *Sw.—Sweetospathodus*, *Ns.—Neospathodus*, *Nv.—Novispathodus*, *Tr.—Triassospathodus*.

tion (Chen et al., 2015; G. Li et al., 2016) are also included here to reconstruct oceanic redox variation history through the latest Permian to Middle Triassic times. A polished surface (~1 × 1 cm) of each sample was examined for its pyrite content using a scanning electron microscope (SEM; Hitachi SU8000) at the State Key Laboratory of Biogeology and Environmental Geology in Wuhan, China. The framboid size distributions were measured when present, and where possible, a minimum number of 100 pyrite framboid sizes was measured for each sample. Measurement bias may come from overlooking smaller framboids, possibly shifting the spectrum toward larger sizes, but such shifts are compensated for, as framboid diameters tend to be underestimated, because spheres are usually not exactly broken in half (Hethke et al., 2013). Furthermore, the same analytical approach was used for each sample.

Framboidal iron monosulfides are authigenic minerals, found in abundance at the redox interface between the oxic and sulfidic zones in modern environments, that convert to pyrite during burial (Wilkin et al., 1996). In euxinic settings, framboids rarely reach 5–6 m diameter before the dense particles sink to the seabed and accumulate as small-size populations with a narrow size distribution (Wilkin et al., 1996). In dysoxic environments, seafloor conditions are weakly oxygenated, and framboids form within the surface sediments, where their size is governed by the local availability of reactants, with the result that they are more variable and generally larger in size (Wilkin et al., 1996). Criteria based on size distribution and morphology of framboids to distinguish five redox states mainly follows Bond and Wignall (2010). In general, when framboids are small (mean diameters: 3–5 μm), abundant, with a narrow size range, and form the dominant pyrite fraction, they indicate euxinia (a persistently sulfidic lower water column). If framboids are small (mean diameters: 4–6 μm), abundant, with a few, larger forms, and dominate the pyrite fraction, then they indicate anoxic conditions (without oxygen in bottom waters for long periods). When framboids have mean diameters of 6–10 μm and are moderately common, with a few, larger framboids together with crystalline pyrite, then such populations are encountered in lower dysoxic conditions (with weakly oxygenated bottom waters). In upper dysoxic environments (with partial oxygen restriction in bottom waters), framboids are usually still present, (although crystalline pyrite is more abundant) and have a broad range of sizes with only a small proportion of framboids <5 μm. In oxic conditions (without oxygen restriction), no framboids are present, and pyrite crystals occur rarely.

Cross plots of mean framboid size (M) versus standard deviation (SD) can also be employed to interpret redox conditions (L. Tian et al., 2014). On the cross-plot diagram, the boundary separating euxinic from oxic-dysoxic facies was determined by means of the equation: $M = -3.3 \times SD + 14$ (L. Tian et al., 2014). Both Bond and Wignall's (2010) criteria and the M-SD cross-plot diagram (L. Tian et al., 2014) were utilized here to assess the redox history of the ramp settings in South China through the latest Permian to Middle Triassic.

RESULTS AND INTERPRETATION OF REDOX HISTORY

Meishan and West Pingdingshan Section

The redox history in the Meishan section during the Permian-Triassic transition has been well studied based on morphology and size variation of pyrite framboids (Shen et al., 2007; Chen et al., 2015; G. Li et al., 2016). Here, we focus on the layers that have not been sampled before, mainly from Beds 30–56 (*C. planata* zone; Table DR1 see footnote 1]). However, most of these samples yielded rare or no pyrite framboids, and only one sample from Bed 30–2 yielded a few pyrite framboids with mean diameter of 5.43 μm, suggesting dysoxia at this level.

In West Pingdingshan, the framboid distribution is highly variable; 20 of 48 samples yielded a few or abundant pyrite framboids; the rest of the samples had few or no pyrite framboids (Table DR1 [see footnote 1]). The relationship between framboid abundance and lithology is unclear because framboids are found in a range of lithologies, but they are also inconsistently present in samples of the same lithology (Fig. 2). Most framboids in the productive samples have small mean diameters (3–6 μm; Fig. 2) and similarly small standard deviations, with the result that they plot in the euxinic-anoxic spectrum (Fig. 3). The exception is a series of samples from the middle Yinkeng Formation that have much larger maximum framboid size (up to 33.22 μm), which fall into the dysoxic field on the M-SD plot (Fig. 3).

Ten samples were collected from Griesbachian strata, and three of them yielded framboids. The earliest Griesbachian sample with pyrite framboids had populations mostly <5 μm in diameter, indicating euxinic-anoxic conditions. A higher sample (from the upper *C. krystyni* zone, late Griesbachian) was also dominated by

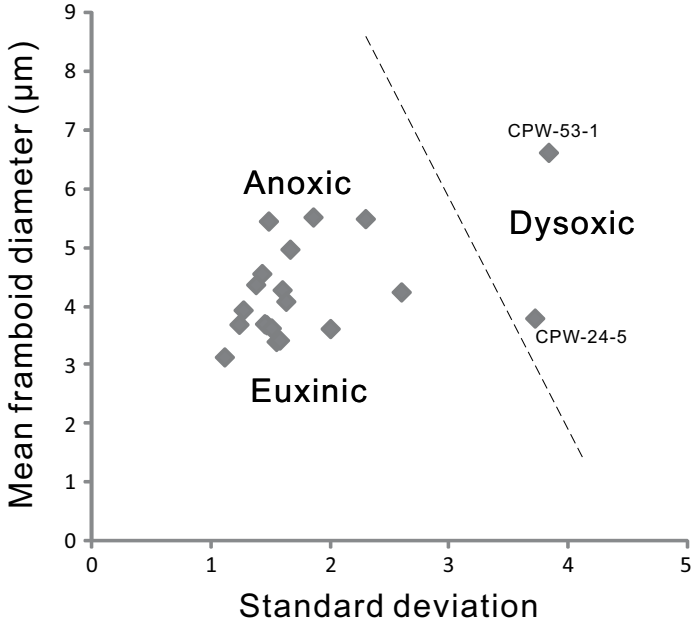

Figure 3. Cross-plot diagram showing mean diameter (M) vs. standard deviation (SD) of pyrite framboid sizes from the West Pingdingshan section. For determination of the dash line separating euxinic/anoxic facies from dysoxic facies, see text (after L. Tian et al., 2014). Note that all samples fall into the anoxic-euxinic field, except for CPW-24-5 (end-Dienerian) and CPW-53-1 (early Spathian), which fall into the dysoxic condition field.

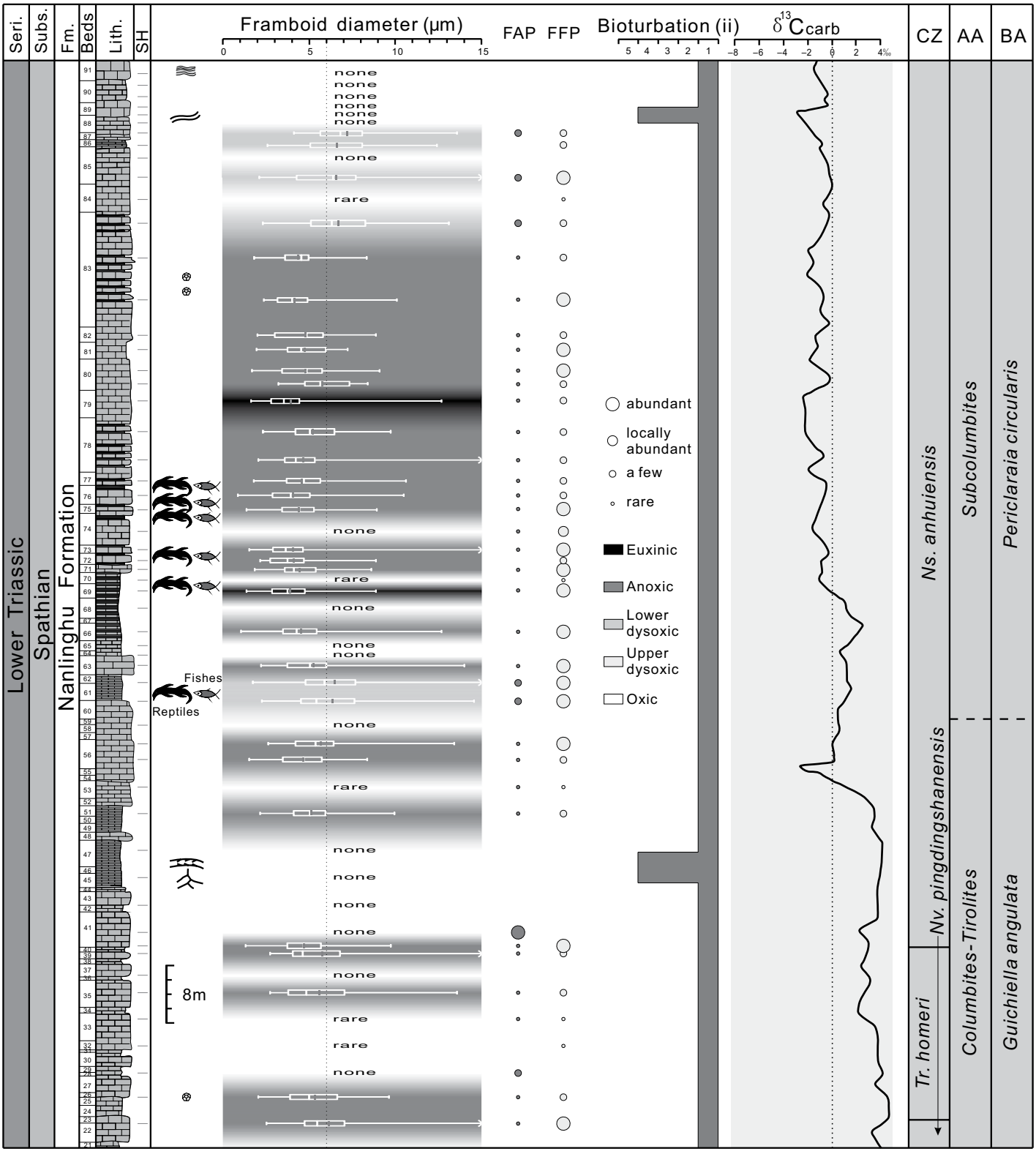

Figure 4. Spathian paleoredox condition variations from the South Majiashan (SMJS) section. Reptile and fish data are from Motani et al. (2014, 2015) and Jiang et al. (2014). For isotopic and paleontologic datum sources, abbreviations, and legends, see Figure 2 (except CZ—conodont zonation). *Tr.—Triassospathodus*, *Nv.—Novispathodus*, *Ns.—Neospathodus*.

tiny framboids, but with rarer larger examples up to 13.5 µm, suggesting an overall lower dysoxic redox regime. Dienerian samples (*Sw. kummeli* to the *Nv. waageni eowaageni* zones) also had tiny, euxinic framboids, but three samples from the Dienerian-Smithian boundary had a much broader framboid size range (with some >15 µm in diameter) that falls in the dysoxic field of the M-SD plot (Fig. 3). Euxinic conditions are then inferred to have returned in the early Smithian, where tiny framboids with a narrow size range reappear.

Above this, in the lower part of *Nv. w. waageni* zone, most samples contained no or few large framboids, indicating well-oxygenated conditions. Redox conditions abruptly returned to euxinia in the middle part of *Nv. w. waageni* zone, where abundant framboids were found, mostly <5 µm in diameter. Samples from across the Smithian-Spathian boundary (defined by the boundary between the upper *Nv. w. waageni* zone and lower *Nv. pingdingshanensis* zones) also yielded abundant tiny framboids. Immediately above the Smithian-Spathian boundary, framboids became very large, and a few pyrite crystals appeared, indicating a dysoxic facies. Only two samples from the upper *Nv. pingdingshanensis* zone and lower *Tr. homeri* zone yielded abundant tiny framboids (<5 µm in diameter), but with a "tail" of larger examples, indicating that the early Spathian waters were likely in a lower dysoxic state.

In summary, the general picture from the West Pingdingshan section shows that redox conditions fluctuated frequently in the Early Triassic, including three relatively long euxinic periods, corresponding to the Griesbachian-Dienerian boundary, early Smithian, and latest Smithian (Fig. 2).

South Majiashan Section

Pyrite framboids are relatively common in the Spathian South Majiashan section (Fig. 4): 32 of 43 samples yielded examples (Table DR1 [see footnote 1]). The M-SD plot (Fig. 5) shows that only two samples fall within the dysoxic field, with the remainder in the euxinic-anoxic field. However, the overall picture (Fig. 4) is one of frequent oscillation of redox conditions, from framboid-free oxic beds to small framboid-rich euxinic beds in the early Spathian, followed by more persistent euxinia in the later Spathian (corresponding to the middle to upper *Ns. anhuiensis* zone). Finally, in the highest beds in this section, belonging to the uppermost *Ns. anhuiensis* zone, framboids are absent, implying oxic conditions. Several of the beds that lack framboids are burrowed. Pelagic fauna (marine reptiles and fish) appear in beds that record a range of redox conditions, although they are most common in euxinic facies, where preservational conditions were optimal (Fig. 4; Motani et al., 2014, 2015; Jiang et al., 2014).

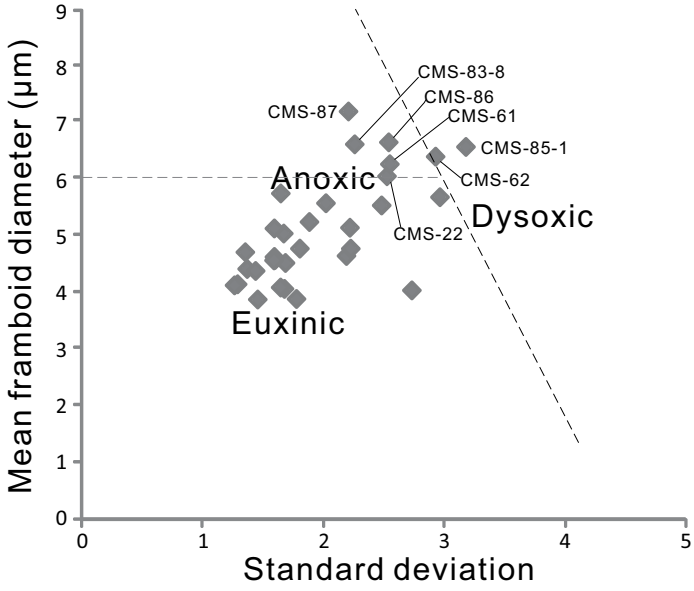

Figure 5. Cross-plot diagram showing mean diameter (M) vs. standard deviation (SD) of pyrite framboid sizes from the South Majiashan (SMJS) section. Note that four samples (CMS-87, CMS-83-8, CMS-86, CMS-61) are plotted in the euxinic-anoxic field but with mean diameter >6 µm.

Qingyan Section

In total, 37 of 88 samples from the uppermost Spathian to uppermost Anisian section at Qingyan yielded pyrite framboids (Fig. 6), with sizes that record a spectrum of redox conditions (Fig. 7). The late Spathian saw a relatively long anoxic-euxinic phase, terminated by a short dysoxic period, and then a relatively long oxic period during the Spathian-Anisian transition (Fig. 6). This is a similar redox history to that recorded in the South Majiashan section (Fig. 4). Noteworthy euxinic episodes in the Anisian are recorded in the Mafengpo Member and the lower Yingshangpo Member (Fig. 7). Interestingly, the lower euxinic-anoxic interval in the latter unit coincides with the presence of microgastropod shell beds, microbialites, and seafloor carbonate precipitates (Z.Q. Chen et al., 2010)—a range of attributes typical of Early Triassic times. In contrast, conditions in the Xiaoshan and Mafengpo Members (early Anisian) were generally well oxygenated. Such conditions are also common in the uppermost Leidapo Member, although the pyrite assemblages from the upper part of this unit suggest dysoxic bottom waters (Fig. 6).

DISCUSSION

Ten-Million-Year Oceanic Redox History from Latest Permian to Early Middle Triassic in South China

Pyrite framboid morphologies and size variations allow recognition of three major euxinic-anoxic episodes from the uppermost Permian to lower Middle Triassic succession in South China (Fig. 8): end-Changhsingian to end-Smithian (episode 1), middle to late Spathian (episode 2), and early to middle Anisian (episode 3). The end-Changhsingian to end-Smithian reducing episode is subdivided into four subepisodes: Permian-Triassic boundary (subepisode 1-a), Griesbachian-Dienerian boundary (subepisode 1-b), earliest Smithian (subepisode 1-c), and end-Smithian (subepisode 1-d) intervals (Fig. 8).

Permian-Triassic Boundary Subepisode

Both sulfur isotopic excursions and biomarker analysis suggest that short periods of euxinic water columns developed at Meishan during the *C. yini* zone (Grice et al., 2005; Shen et al., 2011). Similarly, pyrite framboids also indicate dysoxic conditions due to their large sizes (>6 µm in diameter), with only one very short interval of euxinic-anoxic conditions (Fig. 9; G. Li et al., 2016). Anoxia then devel-

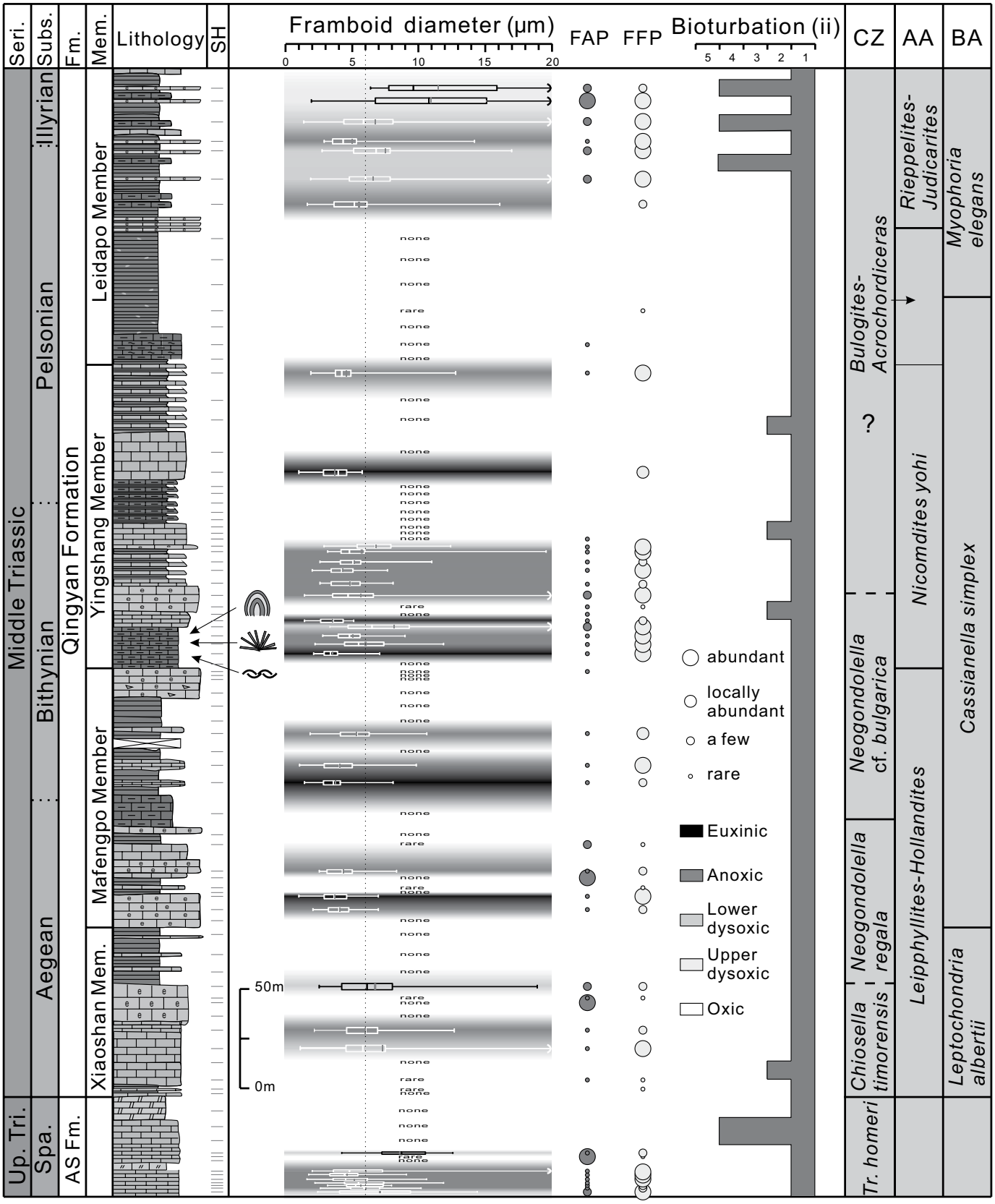

Figure 6. Latest Spathian to late Anisian paleoredox variations from the Qingyan (QY) section. Conodont zonation is after Ji et al. (2011) and Yao et al. (2004), ammonoid assemblage is after Stiller and Bucher (2011, 2008), bivalve assemblage is after J. Chen et al. (2010b). CZ—conodont zonation; AS—Anshun Formation; *Tr.*—*Triassospathodus*. For other abbreviations and legends, see Figure 2.

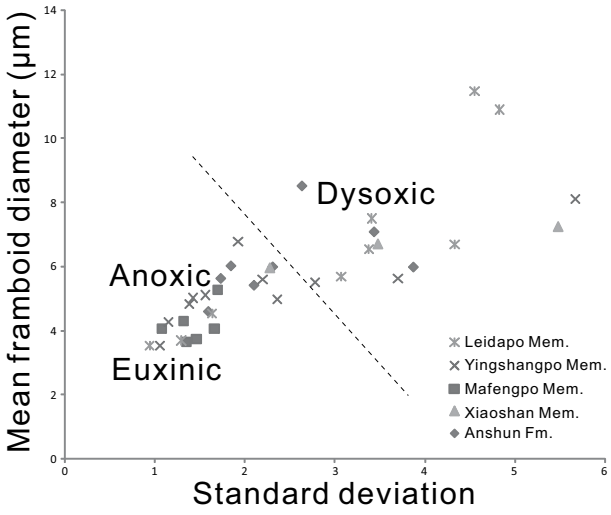

Figure 7. Cross-plot diagram showing mean diameter (M) vs. standard deviation (SD) of pyrite framboid sizes from the Qingyan (QY) section.

oped in the *C. meishanensis* zone (Bed 25; Shen et al., 2007), and a euxinic peak occurred in the *H. changxingensis* zone (Bed 26) and succeeding *C. taylorae* zone (Bed 27b; Chen et al., 2015; this study). No pyrite framboids occur in Bed 27c–d, and large pyrite framboids (8.7 μm in mean diameter) are found in Bed 28, indicating dysoxic to oxic conditions in the *H. parvus* zone and lower *I. staeschei* zone (Bond and Wignall, 2010; this study). Abundant tiny framboids return in Bed 29a–b, implying anoxic conditions in the upper *I. staeschei* zone and *I. isarcica* zone, which persisted, with short interruptions, into the early to middle Griesbachian (Fig. 9; Chen et al., 2015; G. Li et al., 2016).

The two euxinic-anoxic phases in Bed 26–27a and Bed 29a–b coincide closely with metazoan extinction, which occurs at the top of Beds 25 and 28 (H.J. Song et al., 2013). These two euxinic-anoxic peaks coincide with the two microbial blooms bracketed to Beds 26–27a and Bed 29, respectively, in Meishan (Xie et al., 2005). They also correspond to two negative excursions in carbon isotope (Xie et al., 2007) and sulfur isotope values (H.Y. Song et al., 2013), as well as total organic carbon (TOC) concentration peaks from the same section (Fig. 8; Yin et al., 2012). The first reducing phase coincided with a rapid and dramatic 8 °C increase in sea-surface temperature (SST) from Bed 24e to Bed 27a (Sun et al., 2012). The SST remained high (up to 35–39 °C), during the second euxinic-anoxic phase. Accordingly, the first oxygen-poor water-column event may have resulted from the rapid increase in SST, and both factors may have directly killed marine life in the first phase of the Permian-Triassic extinction (H.J. Song et al., 2014). The early to middle Griesbachian redox conditions (*I. isarcica* zone to upper *C. planata* zone) fluctuated frequently (Fig. 9), indicating high-frequency chemocline fluctuations at this time too.

Griesbachian-Dienerian Boundary Subepisode

The presence of small framboids indicates the presence of a Griesbachian-Dienerian boundary euxinic-anoxic interval (Fig. 8). This reducing event is also recorded as a distinct positive conodont Ce anomaly (Song et al., 2012), and it corresponds to a pronounced negative excursion of $\delta^{34}S_{cas}$ (carbonate-associated sulfate) isotopes and $\delta^{13}C_{carb}$ isotopes (Fig. 8). This euxinia-anoxia was also associated with a peak in SSTs (Sun et al., 2012). The Griesbachian-Dienerian transition also saw a dramatic decline in diversity among conodonts and ammonoids (Orchard, 2007; Brayard et al., 2009; Stanley, 2009). Thus, the prevailing euxinic-anoxic water columns over the Griesbachian-Dienerian transition may have been linked with the extinction of pelagic clades such as conodonts and ammonoids that had survived with reasonable success during the Permian-Triassic mass extinction.

Earliest Smithian Subepisode

Following the establishment of generally well-oxygenated conditions in the Dienerian, dysoxia was established at the end of the Dienerian (upper *Ns. dieneri* zone at West Pingdingshan). The anoxia then intensified into a pronounced euxinic-anoxic period in the *Nv. waageni eowaageni* zone. Conodont oxygen isotopes also reveal the onset of a warming trend at this time (Sun et al., 2012). The coeval conodont ΩCe record shows a negative excursion (Fig. 9) that also indicates increasing dysoxia (Song et al., 2012). However, the $\delta^{34}S_{cas}$ isotope record exhibits a turnover from positive to negative excursions, suggesting a global decrease in the amount of pyrite accumulating—an unexpected trend if global anoxia has increased (Fig. 9). It is possible that this brief earliest Smithian anoxic event has not been sampled in the global $\delta^{34}S_{cas}$ record, or the event may be a regional one only manifested in South China.

End-Smithian Subepisode

Pyrite framboid evidence suggests euxinic conditions developed at the end of the Smithian (*Nv. waageni waageni* zone), followed by a slight improvement to dysoxic conditions in the earliest Spathian *Nv. pingdingshanensis* zone. This redox trend shows close parallels in the sea-surface temperature trend, which reached a peak of warmth around the Smithian-Spathian boundary before cooling (Sun et al., 2012). Other indicators of anoxia (conodont ΩCe anomaly and Th/U ratios) also reveal a short-lived but intense anoxic event at this time (Song et al., 2012). The Smithian-Spathian boundary was also marked by a major crisis among conodonts and ammonoids (Orchard, 2007; Stanley, 2009; Brayard et al., 2009). Both $\delta^{34}S_{cas}$ and $\delta^{13}C_{carb}$ isotopes experienced a sharp transition from a negative to positive excursion across the Smithian-Spathian boundary (H.Y. Song et al., 2014; Zhang et al., 2015).

Middle to Late Spathian Episode

This long euxinic-anoxic interval corresponds to the upper *Ns. anhuiensis* zone (also equivalent to the upper part of the regional conodont *Tr. homeri* zone in South China; Zhao et al., 2013) and the upper *Subcolumbites* ammonoid assemblage in South Majiashan (Fig. 5). The upper part of this interval was also detected in the upper *Tr. homeri* zone of the Qingyan section (Ji et al., 2011). The euxinia is also revealed by a contemporaneous, positive conodont ΩCe excursion (Song et al., 2012). This long-period euxinic-anoxic event predates the purported end-Spathian anoxia recognized from biomarker analysis in the same section (Saito et al., 2015). However, this latter event

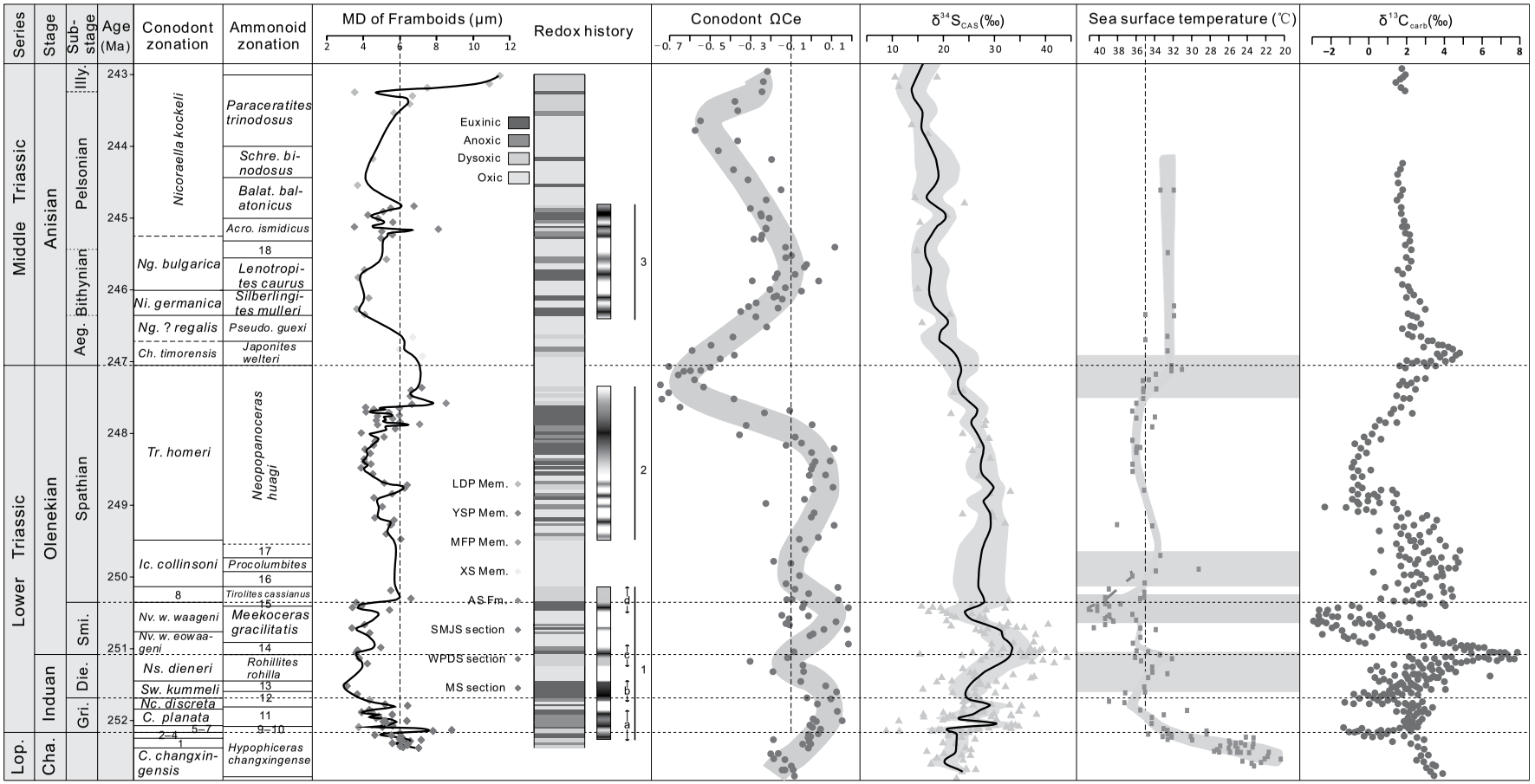

Figure 8. Covariations among pyrite framboid sizes, redox conditions, conodont ΩCe values, sulfur and carbon isotopic excursions, and surface seawater temperatures (SSTs) through the latest Permian to late Anisian (Middle Triassic) from South China. Data sources include: conodont ΩCe (Song et al., 2012), $\delta^{34}S_{cas}$ data (H.Y. Song et al., 2013), SSTs (Sun et al., 2012), carbon isotopes (Payne et al., 2004; Tong et al., 2007). Conodont zones: 1—*Clarkina yini* zone, 2—*Clarkina meishanensis* zone, 3—*Hindeodus changxingensis* zone, 4—*Clarkina taylorae* zone, 5—*Hindeodus parvus* zone, 6—*Isarcicella staeschei* zone, 7—*Isarcicella isarcica* zone, 8—*Novispathodus pingdingshanensis* zone. Ammonoid zones/assemblages: 9—*Otoceras fissisellatum* zone, 10—*Otoceras woodwardi* zone, 11—*Ophiceras tibeticum* zone, 12—*"Pleurogyronites" planidorsatus–Discophiceras* zone, 13—*Rohillites rohilla* zone, 14—*Flemingites flemingianus* zone, 15—*Anawasa tardus* zone, 16—*Columbites parisianus* zone, 17—*Prohungarites-Subcolumbites* zone, 18—*Nicomedites osmani* zone. MD—mean diameter; CAS—carbonate-associated sulfate. Studied sections: LDP—Leidapo; YSP—Yingshangpo; MFP—Mafengpo; XS—Xiaoshan; AS—Anshun; MS—Meishan; WPDS—West Pingdingshan; SMJS—Southern Majiashan. *C.*—*Clarkina*, *Nc.*—*Neoclarkina*, *Sw.*—*Sweetospathodus*, *Ns.*—*Neospathodus*, *Nv.* w.—*Novispathodus waageni*, *Ic.*—*Icriospathodus*, *Tr.*—*Triassospathodus*, *Ch.*—*Chiosella*, *Ng.*—*Neogondolella*, *Ni.*—*Nicoraella*. 1–3—three major euxinic-anoxic episodes, a–d—four euxinic-anoxic sub-episodes in episode 1.

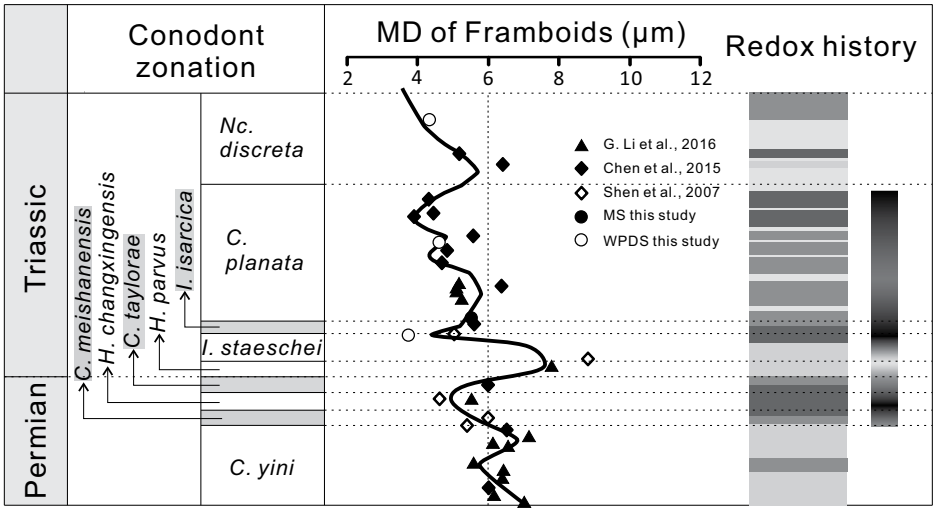

Figure 9. Pyrite framboid size and redox variations through the Permian-Triassic boundary transition spanning from conodont *Clarkina yini* zone to *Neoclarkina discreta* zone. MD—mean diameter. Conodont zones are after Chen et al. (2015), and pyrite framboid size data are after Shen et al. (2007), Chen et al. (2015), G. Li et al. (2016), and this study. Studied sections: MS—Meishan; WPDS—West Pingdingshan. *C.—Clarkina*, *H.—Hindeodus*, *I.—Isarcicella*, *Nc.—Neoclarkina*.

is neither recorded in our data nor in the data of Song et al. (2012), suggesting biomarker evidence alone does not provide a strong criterion for ocean anoxia.

Early to Middle Anisian Episode

Oxygenation levels fluctuated during the entire Anisian, with most frequent euxinic conditions occurring during the Bithynian substage (early–middle Anisian), when three distinct cycles can be recognized (Fig. 8). Each redox cycle consists of two reducing phases interrupted by an abrupt, short oxic phase. Oxygen deficiency overall became less intense up section (Fig. 8). The coeval conodont Ce anomaly data also show dysoxic conditions at this time (Song et al., 2012).

Paleoceanic Redox Variations in Various Paleogeographic Settings and Global Correlations from the Latest Permian to Middle Triassic

Several other studies have attempted to reconstruct the Early and Middle Triassic redox history in other regions (Fig. 10B). Thus, Song et al. (2012) reconstructed the Triassic redox history of a shallow platform margin section in South China based on the ΩCe anomaly record (Fig. 10A). Grasby et al. (2013) reconstructed the Late Permian to Early Triassic redox history of the northwest Pangean Sverdrup Basin, in the Canadian High Arctic, based on pyrite framboid analysis and $\delta^{13}C_{org}$ isotope data obtained from five sections (Fig. 10A). Finally, Wignall et al. (2010) reconstructed the Permian to Jurassic redox history of the Panthalassa Ocean, also based on pyrite framboid analysis from several sections in the Mino-Tamba terrane, Japan (Fig. 10A). In addition to this spatial coverage, variations in redox values with water depth have also been interpreted as movement of the chemocline (Riccardi et al., 2007) or oxygen minimum zone (Algeo et al., 2011b) (Fig. 10C).

Prior to the latest Permian mass extinction in the *C. yini* zone, dysoxic water columns prevailed in both platform margin and ramp settings in South China, and anoxic phases occurred in shallow photic zones elsewhere (Wignall and Twitchett, 1996; Grice et al., 2005; Shen et al., 2011; G. Li et al., 2016; Wignall et al., 2016). Coeval euxinia was also observed in pelagic basins of the Panthalassic Ocean based on framboid, organic carbon isotope, trace-element compositions, and sulfur isotope (Fig. 10C-1) evidence (Wignall et al., 2010; Takahashi et al., 2010, 2013, 2014), although Algeo et al. (2010, 2011b) suggested that the expansion of low-oxygen conditions within the Panthalassic Ocean was focused within the oxygen minimum zone rather than at the deepest seafloor. Coeval euxinia-anoxia was also observed in the deep-water Sverdrup Basin (Algeo et al., 2012; Grasby et al., 2013; Proemse et al., 2013). Knies et al. (2013) further emphasized that the Late Permian euxinic/anoxic seawater of the Sverdrup Basin may have initiated as a midwater oxygen minimum zone rather than on the deep basin floor.

In the main phase of the latest Permian mass extinction and its aftermath, which are bracketed by the *C. meishanensis* and *C. taylorae* zones, euxinic-anoxic conditions have been recognized in all sections from pelagic basin, to deep shelf basin, to ramp to platform margins (Fig. 10C-2). This event therefore swept across the whole ocean from shallow to deep water, implying a huge expansion of the oxygen minimum zone coincident with biotic extinction at that time.

During the *H. parvus* zone, euxinic-anoxic conditions were pronounced in the relatively shallow platform margin (e.g., Guandao section); however, some northwest Pangea shallow-marine sections have yielded unusually diverse Early Triassic ichnofossil assemblages indicating some well-oxygenated refuges (Beatty et al., 2008). Generally, Boreal regions witnessed major oscillations of seafloor oxygenation from oxic to euxinic conditions, even in shallow-water settings (Wignall et al., 2016). The oxygen minimum zone was confined to relatively deep basins and platform margin settings (Fig. 10C-3). In the second phase of the Permian-Triassic mass extinction and its aftermath, equivalent to the *I. staeschei* and *I. isarcica* zones, euxinic-anoxic water columns were pronounced in these settings and basins (Fig. 10C-4).

During the Griesbachian-Dienerian transition, euxinic-anoxic conditions were detected in the relatively deep Sverdrup Basin, and both shallow platform margin and ramp settings, although samples from the Panthalassa Ocean suggest more dysoxic conditions at this time (Fig. 10B; Wignall et al., 2010). Thus, deep-ocean anoxia weakened at this time while remaining intense in shallower settings (Fig. 10C-5).

During the earliest Smithian, euxinic-anoxic water columns can be recognized in ramp settings, whereas dysoxic-oxic conditions prevailed in basins (Fig. 10B). This level has not been sampled in Panthalassan sections, and so the redox values during the early Smithian are unknown.

Euxinic-anoxic conditions expanded dramatically in the late Smithian, although once again, the redox values in the deep ocean have yet to be studied (Fig. 10B). Anoxia expanded into the shallow-water photic zone (platform margin settings) and into ramps and deep-water shelf basins (Fig. 10C-7). Widespread and intense euxinia recurred in the middle–late Spathian but did not coincide with major biotic and climatic changes. This environmental event is widely recognized in all settings and basins (Figs. 10B and 10C-8). In addition, end-Spathian euxinic-anoxic conditions were recognized by biomarker analysis reported from the Panthalassan

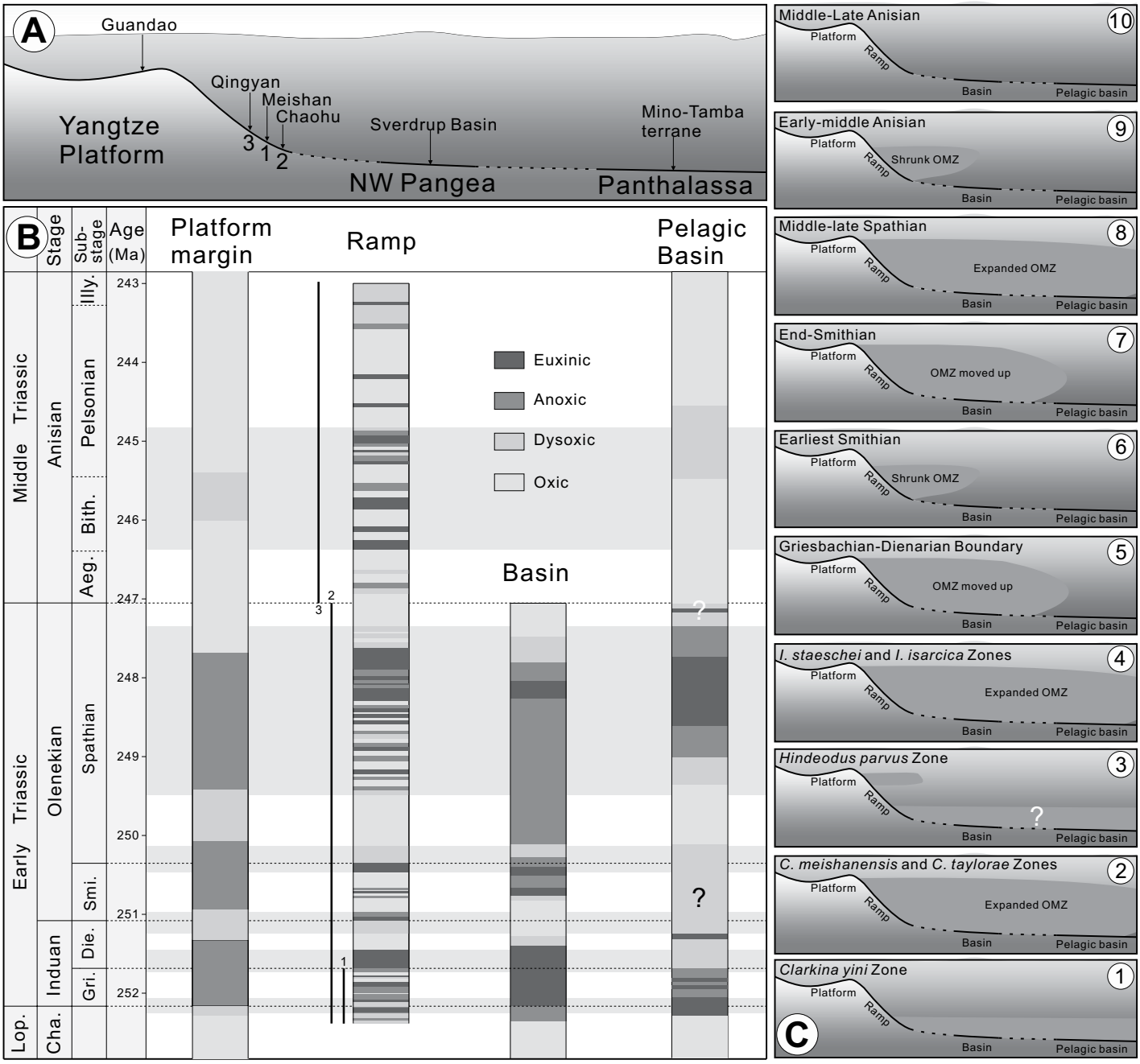

Figure 10. (A) Paleogeographic settings of selected sections studied herein during the latest Permian to Middle Triassic. (B) Global correlations of Early–Middle Triassic redox histories in shallow platform margin and ramp settings of South China, the Sverdrup Basin of Canada, and Mino-Tamba terrane, Japan. (C) Evolution of the oceanic oxygen minimum zone (OMZ; cf. Algeo et al., 2011a) through the entire latest Permian to Middle Triassic. Data sources: Panthalassan ocean of Mino-Tamba terrane, Japan (Wignall et al., 2010) and Momotaro Jinja section, central Japan (Takahashi et al., 2009, 2015), platform margins of South China (Song et al., 2012), Sverdrup Basin of Canada (Grasby et al., 2013), ramp settings of South China (this study). Lop.—Lopingian, Gri.—Griesbachian, Die.—Dienerian, Smi.—Smithian, Aeg.—Aegean, Bith.—Bithynian, Illy.—Illyrian, *C.*—*Clarkina*, *I.*—*Isarcicella*.

sections in Japan (Takahashi et al., 2009, 2015), although this extreme reducing condition was not indicated by pyrite framboids in the sections studied here. The end-Spathian is poorly defined because the last conodont zone of the Early Triassic ranges from the middle to late Spathian in many regions (Zhao et al., 2007). Thus, precise correlation between the Panthalassan and South Chinese sections still remains uncertain. The possibility that the Panthalassan end-Spathian strata are equivalent to the middle to late Spathian of South China cannot be excluded.

During the Anisian, oceans were generally much better oxygenated. However, oxygen-poor conditions became widespread in the middle

part of the stage, especially in ramp settings, suggesting strong oxygen minimum zone development (Fig. 10B). In addition, this interval coincides with the rapid recovery of marine biotas (Chen and Benton, 2012), suggesting that after the frequent and prolonged anoxic events in the Early Triassic, the surviving Middle Triassic animals may have evolved an ability to tolerate oxygen-poor environments to some extent.

CONCLUSIONS

Detailed sampling of pyrite framboid populations has revealed episodic and frequent development of euxinia-anoxia within ramp settings in South China during the latest Permian to Middle Triassic. Three major euxinia-anoxia episodes were recognized in these locations. The longest phase of reducing conditions occurred during the middle to late Spathian. Redox history broadly covaries with positive excursions of conodont ΩCe anomalies, negative excursions of $\delta^{13}C$, negative excursions of $\delta^{34}S_{cas}$, and with peaks in tropical SSTs. The Permian-Triassic boundary oxygen-poor subepisode is resolved into two euxinia-anoxia phases separated by a dysoxic to oxic period; these two euxinic-anoxic phases coincide with two phases of mass extinction on either side of the Permian-Triassic boundary. Global correlations of redox history in different environmental settings and oceanic basins show that three euxinia-anoxia phases (Permian-Triassic boundary, middle to late Spathian, and early to middle Anisian) are widespread and probably occurred globally, although this requires further study in other regions.

ACKNOWLEDGMENTS

We appreciate comments from John Waldon, John-Paul Zonneveld, and an anonymous reviewer that have improved greatly the paper. This study was supported by the 111 Program of China, Ministry of Education of China, two National Natural Science Foundation of China (NSFC) grants (41272023 and 41572091), two research grants from the State Key Laboratory of Biogeology and Environmental Geology (GBL11206), the State Key Laboratory of Geological Processes and Mineral Resources (GPMR201302), China University of Geosciences, and a research grant from Chengdu Center, China Geological Survey (12120113049100). This is a contribution to IGCP 630 (International Geoscience Programme): Permian-Triassic environmental and climatic extremes and biotic responses.

REFERENCES CITED

Algeo, T.J., Ellwood, B., Nguyen, T.K.T., Rowe, H., and Maynard, J.B., 2007, The Permian-Triassic boundary at Nhi Tao, Vietnam: Evidence for recurrent influx of sulfidic watermasses to a shallow-marine carbonate platform: Palaeogeography, Palaeoclimatology, Palaeoecology, v. 252, p. 304–327, doi:10.1016/j.palaeo.2006.11.055.

Algeo, T.J., Shen, Y., Zhang, T., Lyons, T., Bates, S., Rowe, H., and Nguyen, T.K.T., 2008, Association of ^{34}S-depleted pyrite layers with negative carbonate $\delta^{13}C$ excursions at the Permian-Triassic boundary: Evidence for upwelling of sulfidic deep-ocean water masses: Geochemistry, Geophysics, Geosystems, v. 9, p. Q04025, doi:10.1029/2007GC001823.

Algeo, T.J., Hinnov, L., Moser, J., Maynard, J.B., Elswick, E., Kuwahara, K., and Sano, H., 2010, Changes in productivity and redox conditions in the Panthalassic Ocean during the latest Permian: Geology, v. 38, p. 187–190, doi:10.1130/G30483.1.

Algeo, T.J., Chen, Z.Q., Fraiser, M.L., and Twitchett, R.J., 2011a, Terrestrial-marine teleconnections in the collapse and rebuilding of Early Triassic marine ecosystems: Palaeogeography, Palaeoclimatology, Palaeoecology, v. 308, p. 1–11, doi:10.1016/j.palaeo.2011.01.011.

Algeo, T.J., Kuwahara, K., Sano, H., Bates, S., Lyons, T., Elswick, E., Hinnov, L., Ellwood, B., Moser, J., and Maynard, J.B., 2011b, Spatial variation in sediment fluxes, redox conditions, and productivity in the Permian–Triassic Panthalassic Ocean: Palaeogeography, Palaeoclimatology, Palaeoecology, v. 308, p. 65–83, doi:10.1016/j.palaeo.2010.07.007.

Algeo, T.J., Henderson, C.M., Ellwood, B., Rowe, H., Elswick, E., Bates, S., Lyons, T., Hower, J.C., Smith, C., and Maynard, B., 2012, Evidence for a diachronous Late Permian marine crisis from the Canadian Arctic region: Geological Society of America Bulletin, v. 124, p. 1424–1448, doi:10.1130/B30505.1.

Beatty, T.W., Zonneveld, J.P., and Henderson, C.M., 2008, Anomalously diverse Early Triassic ichnofossil assemblages in northwest Pangea: A case for a shallow-marine habitable zone: Geology, v. 36, p. 771–774, doi:10.1130/G24952A.1.

Bond, D.P.G., and Wignall, P.B., 2005, Evidence for Late Devonian (Kellwasser) anoxic events in the Great Basin, western United States, *in* Over, D.J., Morrow, J.R., and Wignall, P.B., eds., Understanding Late Devonian and Permian-Triassic Biotic and Climatic Events: Towards an Integrated Approach: Elsevier Developments in Palaeontology and Stratigraphy 20, p. 225–262.

Bond, D.P.G., and Wignall, P.B., 2010, Pyrite framboid study of marine Permian-Triassic boundary sections: A complex anoxic event and its relationship to contemporaneous mass extinction: Geological Society of America Bulletin, v. 122, p. 1265–1279, doi:10.1130/B30042.1.

Brayard, A., Escarguel, G., Bucher, H., Monnet, C., Bruehwiler, T., Goudemand, N., Galfetti, T., and Guex, J., 2009, Good genes and good luck: Ammonoid diversity and the end-Permian mass extinction: Science, v. 325, p. 1118–1121, doi:10.1126/science.1174638.

Brennecka, G.A., Herrmann, A.D., Algeo, T.J., and Anbar, A.D., 2011, Rapid expansion of oceanic anoxia immediately before the end-Permian mass extinction: Proceedings of the National Academy of Sciences of the United States of America, v. 108, p. 17,631–17,634, doi:10.1073/pnas.1106039108.

Chen, J., Chen, Z.Q., and Tong, J.N., 2010a, Palaeoecology and taphonomy of two brachiopod shell beds from the Anisian (Middle Triassic) of Guizhou, southwest China: Recovery of benthic communities from the end-Permian mass extinction: Global and Planetary Change, v. 73, p. 149–160, doi:10.1016/j.gloplacha.2010.03.012.

Chen, J., Tong, J.N., Niu, Z., Zhou, S., Song, H., and Yi, F., 2010b, Lower–Middle Triassic strata in Qingyan, Guizhou Province, South China: Earth Science, v. 35, p. 51–61 [in Chinese with English abstract], doi:10.3799/dqkx.2010.006.

Chen, Z.Q., and Benton, M.J., 2012, The timing and pattern of biotic recovery following the end-Permian mass extinction: Nature Geoscience, v. 5, p. 375–383, doi:10.1038/ngeo1475.

Chen, Z.Q., Tong, J., Kaiho, K., and Kawahata, H., 2007, Onset of biotic and environmental recovery from the end-Permian mass extinction within 1–2 million years: A case study of the Lower Triassic of the Meishan section, South China: Palaeogeography, Palaeoclimatology, Palaeoecology, v. 252, p. 176–187, doi:10.1016/j.palaeo.2006.11.042.

Chen, Z.Q., Chen, J., Tong, J., and Fraiser, M.L., 2010, Marine ecosystem changes from the latest Permian to Middle Triassic in Qingyan area, Guizhou, southwest China: Journal of Earth Science, v. 21, p. 125–129, doi:10.1007/s12583-010-0187-9.

Chen, Z.Q., Tong, J., and Fraiser, M.L., 2011, Trace fossil evidence for restoration of marine ecosystems following the end-Permian mass extinction in the Lower Yangtze region, South China: Palaeogeography, Palaeoclimatology, Palaeoecology, v. 299, p. 449–474, doi:10.1016/j.palaeo.2010.11.023.

Chen, Z.Q., Yang, H., Luo, M., Benton, M.J., Kaiho, K., Zhao, L., Huang, Y., Zhang, K., Fang, Y., Jiang, H., Qiu, H., Li, Y., Tu, C., Shi, L., Zhang, L., Feng, X., and Chen, L., 2015, Complete biotic and sedimentary records of the Permian-Triassic transition from Meishan section, South China: Ecologically assessing mass extinction and its aftermath: Earth-Science Reviews, v. 149, p. 67–107, doi:10.1016/j.earscirev.2014.10.005.

Dustira, A.M., Wignall, P.B., Joachimski, M., Blomeier, D., Hartkopf-Froeder, C., and Bond, D.P.G., 2013, Gradual onset of anoxia across the Permian-Triassic boundary in Svalbard, Norway: Palaeogeography, Palaeoclimatology, Palaeoecology, v. 374, p. 303–313, doi:10.1016/j.palaeo.2013.02.004.

Erwin, D.H., 2006. Extinction: How Life on Earth Nearly Ended 250 Million Years Ago: Princeton, New Jersey, Princeton University Press, 314 p.

Feng, Z., Bao, Z., and Liu, S., 1997, Lithofacies Palaeogeography of Early and Middle Triassic of South China: Beijing, Petroleum Industry Press, 222 p. [in Chinese]).

Gorjan, P., Kaiho, K., Kakegawa, T., Niitsuma, S., Chen, Z.Q., Kajiwara, Y., and Nicora, A., 2007, Paleoredox, biotic and sulfur-isotopic changes associated with the end-Permian mass extinction in the western Tethys: Chemical Geology, v. 244, p. 483–492, doi:10.1016/j.chemgeo.2007.07.003.

Grasby, S.E., Beauchamp, B., Embry, A., and Sanei, H., 2013, Recurrent Early Triassic ocean anoxia: Geology, v. 41, p. 175–178, doi:10.1130/G33599.1.

Grice, K., Cao, C.Q., Love, G.D., Bottcher, M.E., Twitchett, R.J., Grosjean, E., Summons, R.E., Turgeon, S.C., Dunning, W., and Jin, Y.G., 2005, Photic zone euxinia during the Permian-Triassic superanoxic event: Science, v. 307, p. 706–709, doi:10.1126/science.1104323.

Hallam, A., 1991, Why was there a delayed radiation after the end-Palaeozoic crisis?: Historical Biology, v. 5, p. 257–262, doi:10.1080/10292389109380405.

Hallam, A., and Wignall, P.B., 1997, Mass Extinctions and Their Aftermath: Oxford, UK, Oxford University Press, 320 p.

Hethke, M., Fuersich, F.T., Jiang, B., and Klaus, R., 2013, Oxygen deficiency in Lake Sihetun Formation of the Lower Cretaceous Liaoning Fossillagerstatte (China): Journal of the Geological Society of London, v. 170, p. 817–831, doi:10.1144/jgs2012-102.

Isozaki, Y., 1997, Permo-Triassic boundary superanoxia and stratified superocean: Records from lost deep sea: Science, v. 276, p. 235–238, doi:10.1126/science.276.5310.235.

Ji, W., Tong, J., Zhao, L., Zhou, S., and Chen, J., 2011, Lower–Middle Triassic conodont biostratigraphy of the Qingyan section, Guizhou Province, southwest China: Palaeogeography, Palaeoclimatology, Palaeoecology, v. 308, p. 213–223, doi:10.1016/j.palaeo.2010.08.020.

Jiang, D.Y., Motani, R., Tintori, A., Rieppel, O., Chen, G.-B., Huang, J.-D., Zhang, R., Sun, Z.-Y., and Ji, C., 2014, The Early Triassic eosauropterygian *Majiashanosaurus discocoracoidis*, gen. et sp. Nov. (Reptilia, Sauropterygia), from Chaohu, Anhui Province, People's Republic of China: Journal of Vertebrate Paleontology, v. 34, p. 1044–1052, doi:10.1080/02724634.2014.846264.

Jiang, H., Lai, X., Luo, G., Aldridge, R., Zhang, K., and Wignall, P., 2007, Restudy of conodont zonation and evolution across the P/T boundary at Meishan section, Changxing, Zhejiang, China: Global and Planetary Change, v. 55, p. 39–55, doi:10.1016/j.gloplacha.2006.06.007.

Kaiho, K., Kajiwara, Y., Chen, Z.Q., and Goljan, P., 2006, A sulfur isotope event at the end of the Permian: Chemical Geology, v. 235, p. 33–47, doi:10.1016/j.chemgeo.2006.06.001.

Kaiho, K., Oba, M., Fukuda, Y., Ito, K., Ariyoshi, S., Gorjan, P., Riu, Y., Takahashi, S., Chen, Z.Q., Tong, J., and Yamakita, S., 2012, Changes in depth-transect redox conditions spanning the end-Permian mass extinction and their impact on the marine extinction: Evidence from biomarkers and sulfur isotopes: Global and Planetary Change, v. 94–95, p. 20–32, doi:10.1016/j.gloplacha.2012.05.024.

Knies, J., Grasby, S.E., Beauchamp, B., and Schubert, C.J., 2013, Water mass denitrification during the latest Permian extinction in the Sverdrup Basin, Arctic Canada: Geology, v. 41, p. 167–170, doi:10.1130/G33816.1.

Knoll, A.H., Barnbach, R.K., Payne, J.L., Pruss, S., and Fischer, W.W., 2007, Paleophysiology and end-Permian mass extinction: Earth and Planetary Science Letters, v. 256, p. 295–313, doi:10.1016/j.epsl.2007.02.018.

Li, G., Wang, Y., Shi, G.R., Liao, W., and Yu, L., 2016, Fluctuations of redox condition across the Permian-Triassic boundary—New evidence from the GSSP section in Meishan of South China: Palaeogeography, Palaeoclimatology, Palaeoecology, v. 448, p. 48–58, doi:10.1016/j.palaeo.2015.09.050.

Li, M., Ogg, J., Zhang, Y., Huang, C., Hinnov, L., Chen, Z.Q., and Zou, Z., 2016, Astronomical tuning of the end-Permian extinction and the Early Triassic Epoch of South China and Germany: Earth and Planetary Science Letters, v. 441, p. 10–25, doi:10.1016/j.epsl.2016.02.017.

Lüning, S., Kolonic, S., Loydell, D., and Craig, J., 2003, Reconstruction of the original organic richness in weathered Silurian shale outcrops (Murzuq and Kufra Basins, southern Libya): GeoArabia, v. 8, p. 299–308.

Motani, R., Jiang, D., Tintori, A., Rieppel, O., and Chen, G., 2014, Terrestrial origin of viviparity in Mesozoic marine reptiles indicated by Early Triassic embryonic fossils: PLoS One, v. 9, no. 2, p. e88640, doi:10.1371/journal.pone.0088640.

Motani, R., Jiang, D.Y., Chen, G.B., Tintori, A., Rieppel, O., Ji, C., and Huang, J.D., 2015, A basal ichthyosauriform with a short snout from the Lower Triassic of China: Nature, v. 517, p. 485–488, doi:10.1038/nature13866.

Newton, R.J., Pevitt, E.L., Wignall, P.B., and Bottrell, S.H., 2004, Large shifts in the isotopic composition of seawater sulphate across the Permo-Triassic boundary in northern Italy: Earth and Planetary Science Letters, v. 218, p. 331–345, doi:10.1016/S0012-821X(03)00676-9.

Orchard, M.J., 2007, Conodont diversity and evolution through the latest Permian and Early Triassic upheavals: Palaeogeography, Palaeoclimatology, Palaeoecology, v. 252, p. 93–117, doi:10.1016/j.palaeo.2006.11.037.

Payne, J.L., and Clapham, M.E., 2012, End-Permian mass extinction in the oceans: An ancient analog for the twenty-first century?: Annual Review of Earth and Planetary Sciences, v. 40, p. 89–111, doi:10.1146/annurev-earth-042711-105329.

Payne, J.L., Lehrmann, D.J., Wei, J., Orchard, M.J., Schrag, D.P., and Knoll, A.H., 2004, Large perturbations of the carbon cycle during recovery from the end-Permian extinction: Science, v. 305, p. 506–509, doi:10.1126/science.1097023.

Proemse, B.C., Grasby, S.E., Wieser, M.E., Mayer, B., and Beauchamp, B., 2013, Molybdenum isotopic evidence for oxic marine conditions during the latest Permian extinction: Geology, v. 41, p. 967–970, doi:10.1130/G34466.1.

Riccardi, A.L., Arthur, M.A., and Kump, L.R., 2006, Sulfur isotopic evidence for chemocline upward excursions during the end-Permian mass extinction: Geochimica et Cosmochimica Acta, v. 70, p. 5740–5752, doi:10.1016/j.gca.2006.08.005.

Riccardi, A.L., Kump, L.R., Arthur, M.A., and D'Hondt, S., 2007, Carbon isotopic evidence for chemocline upward excursions during the end-Permian event: Palaeogeography, Palaeoclimatology, Palaeoecology, v. 248, p. 73–81, doi:10.1016/j.palaeo.2006.11.010.

Romano, C., Goudemand, N., Vennemann, T.W., Ware, D., Schneebeli-Hermann, E., Hochuli, P.A., Bruehwiler, T., Brinkmann, W., and Bucher, H., 2013, Climatic and biotic upheavals following the end-Permian mass extinction: Nature Geoscience, v. 6, p. 57–60, doi:10.1038/ngeo1667.

Saito, R., Kaiho, K., Oba, M., Fujibayashi, M., Tong, J., and Tian, L., 2015, Predominance of archaea-derived hydrocarbons in an Early Triassic microbialite: Organic Geochemistry, v. 85, p. 66–75, doi:10.1016/j.orggeochem.2015.05.004.

Schoepfer, S., Shen, J., Wei, H., Tyson, R., Ingall, E., and Algeo, T., 2015, Total organic carbon, organic phosphorus, and biogenic barium fluxes as proxies for paleomarine productivity: Earth-Science Reviews, v. 149, p. 23–52, doi:10.1016/j.earscirev.2014.08.017.

Shen, J., Schoepfer, S.D., Feng, Q., Zhou, L., Yu, J., Song, H., Wei, H., and Algeo, T.J., 2015, Marine productivity changes during the end-Permian crisis and Early Triassic recovery: Earth-Science Reviews, v. 149, p. 136–162, doi:10.1016/j.earscirev.2014.11.002.

Shen, W., Lin, Y., Xu, L., Li, J., Wu, Y., and Sung, Y., 2007, Pyrite framboids in the Permian-Triassic boundary section at Meishan, China: Evidence for dysoxic deposition: Palaeogeography, Palaeoclimatology, Palaeoecology, v. 253, p. 323–331, doi:10.1016/j.palaeo.2007.06.005.

Shen, Y.A., Farquhar, J., Zhang, H., Masterson, A., Zhang, T., and Wing, B.A., 2011, Multiple S-isotopic evidence for episodic shoaling of anoxic water during Late Permian mass extinction: Nature Communications, v. 2, p. 210, doi:10.1038/ncomms1217.

Song, H.J., Wignall, P.B., Tong, J., Bond, D.P.G., Song, H., Lai, X., Zhang, K., Wang, H., and Chen, Y., 2012, Geochemical evidence from bio-apatite for multiple oceanic anoxic events during Permian-Triassic transition and the link with end-Permian extinction and recovery: Earth and Planetary Science Letters, v. 353–354, p. 12–21, doi:10.1016/j.epsl.2012.07.005.

Song, H.J., Wignall, P.B., Chu, D., Tong, J., Sun, Y., Song, H., He, W., and Tian, L., 2014, Anoxia/high temperature double whammy during the Permian-Triassic marine crisis and its aftermath: Scientific Reports, v. 4, p. 4132, doi:10.1038/srep04132.

Song, H.Y., Tong, J., Algeo, T.J., Horacek, M., Qiu, H., Song, H., Tian, L., and Chen, Z.Q., 2013, Large vertical $\delta^{13}C$ gradients in Early Triassic seas of the South China craton: Implications for oceanographic changes related to Siberian Traps volcanism: Global and Planetary Change, v. 105, p. 7–20, doi:10.1016/j.gloplacha.2012.10.023.

Song, H.Y., Tong, J., Algeo, T.J., Song, H., Qiu, H., Zhu, Y., Tian, L., Bates, S., Lyons, T.W., Luo, G., and Kump, L.R., 2014, Early Triassic seawater sulfate drawdown: Geochimica et Cosmochimica Acta, v. 128, p. 95–113, doi:10.1016/j.gca.2013.12.009.

Stanley, S.M., 2009, Evidence from ammonoids and conodonts for multiple Early Triassic mass extinctions: Proceedings of the National Academy of Sciences of the United States of America, v. 106, p. 15,264–15,267, doi:10.1073/pnas.0907992106.

Stiller, F., and Bucher, H., 2008, Anisian ammonoids from Qingyan, southwestern China; biostratigraphical implications for the age of the Qingyan Formation: Swiss Journal of Geosciences, v. 101, p. 547–562, doi:10.1007/s00015-008-1274-0.

Stiller, F., and Bucher, H., 2011, Precise biostratigraphical correlation and age of the Leidapo fossil assemblages early Middle Triassic of Qingyan: Southwest China: Acta Palaeontological Sinica, v. 50, no. 1, p. 1–12.

Sun, Y., Joachimski, M.M., Wignall, P.B., Yan, C., Chen, Y., Jiang, H., Wang, L., and Lai, X., 2012, Lethally hot temperatures during the Early Triassic greenhouse: Science, v. 338, p. 366–370, doi:10.1126/science.1224126.

Takahashi, S., Oba, M., Kaiho, K., Yamakita, S., and Sakata, S., 2009, Panthalassic oceanic anoxia at the end of the Early Triassic: A cause of delay in the recovery of life after the end-Permian mass extinction: Palaeogeography, Palaeoclimatology, Palaeoecology, v. 274, p. 185–195, doi:10.1016/j.palaeo.2009.01.010.

Takahashi, S., Kaiho, K., Oba, M., and Kakegawa, T., 2010, A smooth negative shift of organic carbon isotope ratios at an end-Permian mass extinction horizon in central pelagic Panthalassa: Palaeogeography, Palaeoclimatology, Palaeoecology, v. 292, p. 532–539, doi:10.1016/j.palaeo.2010.04.025.

Takahashi, S., Kaiho, K., Hori, R., Gorjan, P., Watanabe, T., Yamakita, S., Aita, Y., Takemura, A., Sporli, K., and Kakegawa, T., 2013, Sulfur isotope profiles in the pelagic Panthalassic deep sea during the Permian-Triassic transition: Global and Planetary Change, v. 105, p. 68–78, doi:10.1016/j.gloplacha.2012.12.006.

Takahashi, S., Yamasaki, S., Ogawa, K., Kimura, K., Kaiho, K., Yoshida, T., and Tsuchiya, N., 2014, Bioessential element-depleted ocean following the euxinic maximum of the end-Permian mass extinction: Earth and Planetary Science Letters, v. 393, p. 94–104, doi:10.1016/j.epsl.2014.02.041.

Takahashi, S., Yamasaki, S., Ogawa, K., Kaiho, K., and Tsuchiya, N., 2015, Redox conditions in the end–Early Triassic Panthalassa: Palaeogeography, Palaeoclimatology, Palaeoecology, v. 432, p. 15–28, doi:10.1016/j.palaeo.2015.04.018.

Tian, L., Tong, J., Algeo, T.J., Song, H., Song, H., Chu, D., Shi, L., and Bottjer, D.J., 2014, Reconstruction of Early Triassic ocean redox conditions based on framboidal pyrite from the Nanpanjiang Basin, South China: Palaeogeography, Palaeoclimatology, Palaeoecology, v. 412, p. 68–79, doi:10.1016/j.palaeo.2014.07.018.

Tian, S.F., Chen, Z.Q., and Huang, C., 2014, Orbital forcing and sea-level changes in the earliest Triassic of the Meishan section, South China: Journal of Earth Science, v. 25, p. 64–73, doi:10.1007/s12583-014-0400-3.

Tong, J., Zakharov, Y.D., Orchard, M.J., Yin, H.F., and Hansen, H.J., 2003, A candidate for the Induan-Olenekian boundary stratotype in the Tethyan region: Science in China, ser. D, Earth Sciences, v. 46, p. 1182–1200, doi:10.1360/03yd0295.

Tong, J., Zakharov, Y.D., and Wu, S.B., 2004, Early Triassic ammonoid succession in Chaohu, Anhui Province: Acta Palaeontologica Sinica, v. 43, p. 192–204 [in Chinese with English abstract].

Tong, J., Zuo, J., and Chen, Z.Q., 2007, Early Triassic carbon isotope excursions from South China: Proxies for devastation and restoration of marine ecosystems following the end-Permian mass extinction: Geological Journal, v. 42, p. 371–389, doi:10.1002/gj.1084.

Wignall, P.B., 2015, The Worst of Times: How Life on Earth Survived Eighty Million Years of Extinctions: Princeton, New Jersey, Princeton University Press, 199 p., doi:10.1515/9781400874248.

Wignall, P.B., and Newton, R., 2003, Contrasting deep-water records from the Upper Permian and Lower Triassic of South Tibet and British Columbia: Evidence for a diachronous mass extinction: Palaios, v. 18, p. 153–167, doi:10.1669/0883-1351(2003)18<153:CDRFTU>2.0.CO;2.

Wignall, P.B., and Twitchett, R.J., 1996, Oceanic anoxia and the end Permian mass extinction: Science, v. 272, p. 1155–1158, doi:10.1126/science.272.5265.1155.

Wignall, P.B., and Twitchett, R.J., 2002, Extent, duration, and nature of the Permian-Triassic superanoxic event, *in* Koeberl, C., and MacLeod, K.G., eds., Catastrophic Events and Mass Extinctions: Impacts and Beyond: Geological Society of America Special Paper 356, p. 395–413, doi:10.1130/0-8137-2356-6.395.

Wignall, P.B., Bond, D.P.G., Kuwahara, K., Kakuwa, Y., Newton, R.J., and Poulton, S.W., 2010, An 80 million year oceanic redox history from Permian to Jurassic pelagic sediments of the Mino-Tamba terrane, SW Japan, and the origin of four mass extinctions: Global and Planetary Change, v. 71, p. 109–123, doi:10.1016/j.gloplacha.2010.01.022.

Wignall, P.B., Bond, D.P.G., Sun, Y.-D., Grasby, S.E., Beauchamp, B., Joachimski, M.M., and Blomeier, D.G., 2016, Ultra-shallow marine anoxia in an Early Triassic shallow-marine clastic ramp (Spitsbergen) and the suppression of benthic radiation: Geological Magazine, v. 153, p. 316–331, doi:10.1017/S0016756815000588.

Wilkin, R.T., Barnes, H.L., and Brantley, S.L., 1996, The size distribution of framboidal pyrite in modern sediments: An indicator of redox conditions: Geochimica et Cosmochimica Acta, v. 60, p. 3897–3912, doi:10.1016/0016-7037(96)00209-8.

Xie, S., Pancost, R.D., Yin, H.F., Wang, H.M., and Evershed, R.P., 2005, Two episodes of microbial change coupled with Permo/Triassic faunal mass extinction: Nature, v. 434, p. 494–497, doi:10.1038/nature03396.

Xie, S., Pancost, R.D., Huang, J., Wignall, P.B., Yu, J., Tang, X., Chen, L., Huang, X., and Lai, X., 2007, Changes in the global carbon cycle occurred as two episodes during the Permian-Triassic crisis: Geology, v. 35, p. 1083–1086, doi:10.1130/G24224A.1.

Yan, C., Jiang, H., Lai, X., Sun, Y., Yang, B., and Wang, L., 2015, The relationship between the "Green-Bean Rock" layers and conodont *Chiosella timorensis* and implications on defining the Early-Middle Triassic boundary in the Nanpanjiang Basin, South China: Journal of Earth Science, v. 26, p. 236–245, doi:10.1007/s12583-015-0535-x.

Yao, J., Ji, Z., Wang, L., and Wu, G., 2004, Research on conodont biostratigraphy near the bottom boundary of the Middle Triassic Qingyan Stage in the southern Guizhou Province: Acta Geologica Sinica, v. 78, p. 577–587 [in Chinese].

Yin, H., Zhang, K., Tong, J., Yang, Z., and Wu, S., 2001, The global stratotype section and point (GSSP) of the Permian-Triassic boundary: Episodes, v. 24, p. 102–114.

Yin, H., Xie, S., Luo, G., Algeo, T.J., and Zhang, K., 2012, Two episodes of environmental change at the Permian-Triassic boundary of the GSSP section Meishan: Earth-Science Reviews, v. 115, p. 163–172, doi:10.1016/j.earscirev.2012.08.006.

Zhang, K., Tong, J., Shi, G.R., Lai, X., Yu, J., He, W., Peng, Y., and Jin, Y., 2007, Early Triassic conodont-palynological biostratigraphy of the Meishan D section in Changxing, Zhejiang Province, South China: Palaeogeography, Palaeoclimatology, Palaeoecology, v. 252, p. 4–23, doi:10.1016/j.palaeo.2006.11.031.

Zhang, L., Zhao, L., Chen, Z.Q., Algeo, T.J., Li, Y., and Cao, L., 2015, Amelioration of marine environments at the Smithian-Spathian boundary, Early Triassic: Biogeosciences, v. 12, p. 1597–1613, doi:10.5194/bg-12-1597-2015.

Zhang, N., Jiang, H., and Zhong, W., 2014, Conodont biostratigraphy across the Permian-Triassic boundary at the Xinmin section, Guizhou, South China: Journal of Earth Science, v. 25, p. 779–786, doi:10.1007/s12583-014-0472-0.

Zhao, L., Orchard, M.J., Tong, J., Sun, Z., Zuo, J., Zhang, S., and Yun, A., 2007, Lower Triassic conodont sequence in Chaohu, Anhui Province, China, and its global correlation: Palaeogeography, Palaeoclimatology, Palaeoecology, v. 252, p. 24–38, doi:10.1016/j.palaeo.2006.11.032.

Zhao, L., Tong, J., Zhang, S., and Sun, Z., 2008, An update of conodonts in the Induan-Olenekian boundary strata at west Pingdingshan section, Chaohu: Anhui Province: Journal of China University of Geosciences, v. 19, p. 207–216, doi:10.1016/S1002-0705(08)60040-0.

Zhao, L., Chen, Y., Chen, Z.Q., and Cao, L., 2013, Uppermost Permian to Lower Triassic conodont zonation from Three Gorges area, South China: Palaios, v. 28, p. 523–540, doi:10.2110/palo.2012.p12-107r.

Zhou, L., Wignall, P.B., Su, J., Feng, Q., Xie, S., Zhao, L., and Huang, J., 2012, U/Mo ratios and delta Mo-98/95 as local and global redox proxies during mass extinction events: Chemical Geology, v. 324–325, p. 99–107, doi:10.1016/j.chemgeo.2012.03.020.

Science Editor: Christian Koeberl
Associate Editor: John Waldron

Manuscript Received 19 November 2015
Revised Manuscript Received 22 June 2016
Manuscript Accepted 9 September 2016

Printed in the USA